DOI: 10.21062/mft.2025.079 http://www.journalmt.com

Formation of TiO_2 Hollow Nanoparticles Studied by in Situ TEM

Nikoleta Štaffenová (0009-0006-9366-0666)*, Lucia Bajtošová (0000-0002-4746-9231), Elena Chochoľaková (0009-0002-6585-531X), Jan Hanuš (0000-0002-5825-8536), Miroslav Cieslar (0000-0002-2801-3810)
Charles University, Faculty of Mathematics and Physics, Ke Karlovu 3, 12116 Prague, Czech Republic.
*E-mail: lucia.bajtosova@matfyz.cuni.cz

Hollow TiO_2 architectures are attractive for catalysis and sensing but typically produced by wet-chemical templating and sub-micron sizes. Here we demonstrate a dry, template-free route to nanoscale hollow shells by combining DC magnetron sputtering with in situ TEM heating. Heating to 900 °C produces sub-50 nm TiO_2 hollow shells with ~20 nm compact walls via oxidation-driven Kirkendall hollowing. The oxide evolves from amorphous at low temperature to anatase locally (~500 °C) and then to a rutile/brookite mixture by ~600 °C. The hollow architecture withstands a temperature of 900 °C without measurable sintering. Beam-off regions and ex-situ air annealing show the same hollowing and phase evolution, confirming a thermally driven, not beam-induced, transformation reproducible in air.

Keywords: Hollow TiO_2, Rutile/brookite, Magnetron sputtering, in situ TEM, Kirkendall effect

1 Introduction

In recent years, hollow inorganic spheres spanning nanometer to micrometer dimensions have attracted significant attention due to their unique structural characteristics and broad application potential. Such shell-type architectures have been investigated for use in drug delivery, product encapsulation, or protein and enzyme transplantation [1-3].

Titanium dioxide (TiO_2) is widely regarded as an auspicious material in numerous scientific and technological fields [4]. This is due to its favorable properties—namely, catalytic activity [5], photocatalysis [6, 7], and photoelectrochemical conversion [8]. Moreover, the catalytic activity and electrical properties of TiO_2 are susceptible to its morphology and crystalline phase [9, 10]. TiO_2 has three main allotropic modifications—rutile, anatase, and brookite [11]. Several recent studies have reported the fabrication of hollow TiO_2 shells with well-defined cavities to enhance photocatalytic activity or other properties. For this, number of routes have been explored, including polystyrene (PS) colloidal sphere templating [12]; sol–gel condensation of titanium hydroxide [13]; hard-templating with removable cores followed by etching/calcination [14]; soft-templating with surfactant/block-copolymer micelles [15], microemulsions [16], or Pickering emulsions [17]; aerosol/spray methods [18]; gas-bubble templating [19]; self-templating via Ostwald ripening [20] and the Kirkendall effect [21]; layer-by-layer assembly on colloids with core removal [22]; conformal coating by ALD/CVD on sacrificial particles [23]; hydro/solvothermal corrosion of titanates [24]; and (co)axial electrospinning to form hollow fibers/shells [25].

In many templated and aerosol routes, the resulting hollow TiO_2 shells are mostly submicron to micron in diameter (≈0.2–1 μm) [1, 12, 14, 18]. Reducing the particle size can be advantageous for applications requiring high surface area, shortened ion/electron transport pathways, and enhanced electrochemical performance. Prior reports have achieved sub-20 nm hollow TiO_2 particles—often anatase/ TiO_2 (B)—using solution-based Ostwald or Kirkendall routes [26, 27], as well as microemulsion-based synthesis [28]. However, these routes frequently produce ultrathin, porous walls prone to sintering, pore collapse, and phase-change–induced cracking during thermal treatment. Here we adopt a physical-vapor route: magnetron sputtering to form hcp-Ti cores with a TiO_x shell, followed by annealing up to 950 °C. The thermal step drives oxidation-induced (Kirkendall-type) hollowing, converting the Ti core into a void and the TiO_x shell into crystalline TiO_2 hollow shells with <50 nm outer diameter and ~20 nm thick walls. The shells crystallize as a brookite/rutile mixture and retain their hollow architecture after brief anneals up to 950 °C.

2 Methods

A primary gas aggregation cluster source (GAS) was used for producing Ti NPs, using current of 400 mA, corresponding to a power of 66 W and a voltage of 164 V. Argon was introduced at a constant flow rate of 5 sccm. The working pressure was maintained at 48 Pa. Upon exposure to air after deposition, the surface of the Ti NPs oxidized spontaneously, resulting in the formation of a TiO_2 shell surrounding the Ti core.

For TEM analysis, the NPs were detached from the glass substrate using a razor blade, dispersed in methanol, and subsequently pipetted onto a TEM grid coated with ultrathin silicon dioxide (SiO_2) support film.

The specimens were examined using a JEOL 2200FS transmission electron microscope operated in both TEM and STEM modes at 200 kV. The characterization included high-resolution TEM (HRTEM), energy-dispersive X-ray spectroscopy (EDX), bright-field (BF), high-angle annular dark-field (HAADF), and secondary electron (SE) imaging.

3 Results and discussion

Figure 1 presents characteristic images of the prepared samples. The nanoparticles are predominantly spherical or hexagonal in shape, with an average diameter of 50 nm. They display a clear core–shell morphology, with an average shell thickness of 5 nm. Energy-dispersive X-ray spectroscopy (EDS) mapping (Figure 1d-f) confirms the presence of a Ti-rich core surrounded by an oxidized Ti shell.

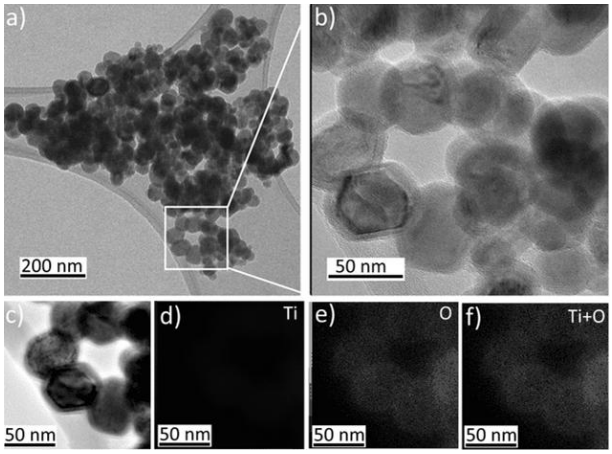

Fig. 1 *As sputtered nanoparticles, a) TEM BF, b) STEM BF, with corresponding EDS maps d-f)*

The structure was further examined by HRTEM. Figure 2 presents a detailed analysis of a well-oriented nanoparticle. The fast Fourier transform (FFT) of the HRTEM image confirms the presence of an hcp Ti core surrounded by an amorphous shell.

The sample was annealed up to 300 °C, 600 °C, then in 100 °C increments up to 800 °C and 50 °C increments up to 900 °C. Each temperature was maintained for 10 minutes. The evolution of the microstructure with increasing temperature is shown in Figure 3. Up to 850 °C, the particles retained their size and shape with no evidence of neck formation or particle coalescence. Sintering of a few particles (highlighted in Figure 3f) at 900 °C was observed; however, this represented a minor deviation from the overall trend. A pronounced shell becomes evident at 600 °C, followed by partial shell separation at 700 °C. From 800 °C onward, voids form and grow progressively with increasing temperature.

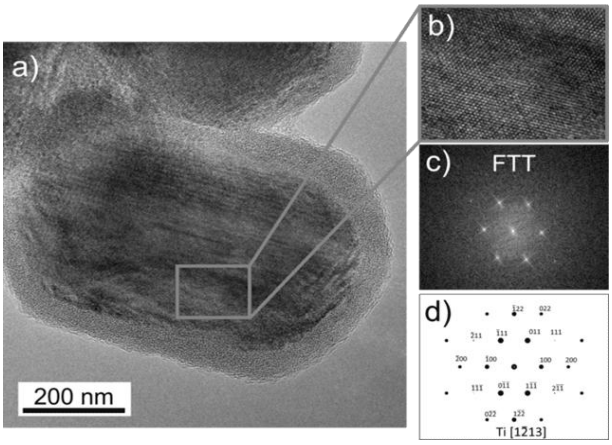

Fig. 2 *Details of the initial state, a) HRTEM, b) FFT of highlighted area in a), c) simulated image of HCP Ti, d) overlay of b) and c)*

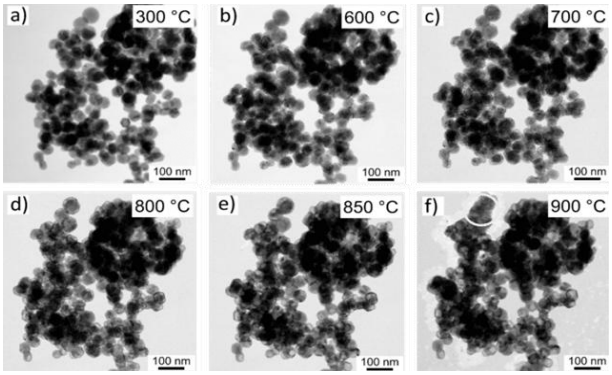

Fig. 3 *STEM BF images of the nanoparticles annealed to temperatures 300 – 900 °C*

At 600 °C, the onset of the core–shell separation is evident (Figure 4): the shell thickens from ≈4 nm to ≈5 nm, the core shrinks from ≈45 nm to ≈43 nm, and a distinct gap forms between them. The crystalline nature of the oxide shell was further investigated by HRTEM (Figure 5a), FFT analysis (Figure 5b–d) confirms that the initially amorphous oxide shell crystallizes to rutile in this temperature window. The selected area diffraction taken from the cluster of nanoparticles after annealing (Figure 5e) also shows the evidence of brookite phase, particularly in (200) and (211) rings, pointing to a mixed rutile/brookite shell.

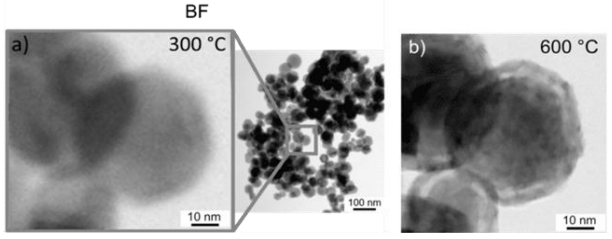

Fig. 4 *STEM BF images of the nanoparticles annealed to temperatures 300 – 900 °C*

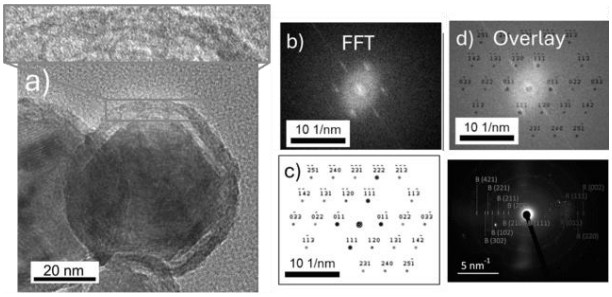

Fig. 5 *a) HRTEM image of the transformed shell at 600 °C, b) FFT of the highlighted area in a), c) simulated image of HCP Ti, d) overlay of b) and c), e) SAED diffraction taken from a larger area after annealing*

The gradual development of a thin gap between the metallic core and the oxide shell leads to the formation of fully hollow shells in some nanoparticles at higher temperatures (Figure 3d-f). Detailed images in Figure 6c,d) reveal a noticeable thickening of the oxide shell with increasing temperature. When the metallic Ti oxidizes to rutile, the volume expands by a factor of ~1.78 due to the lower density of TiO_2 compared to Ti. In our case, the Ti core (22 nm radius) with a thin separated shell at 600 °C transforms into a thicker shell at 900 °C. The measured increase in shell volume ($\sim 1.0 \times 10^4$ nm^3) closely matches the volume of rutile expected from complete oxidation of the Ti core ($\sim 9.9 \times 10^3$ nm^3). This agreement indicates that the observed structural change is consistent with the Ti → TiO_2 volume transformation, suggesting that the metallic Ti core has progressively diffused into the shell to form a growing oxide layer.

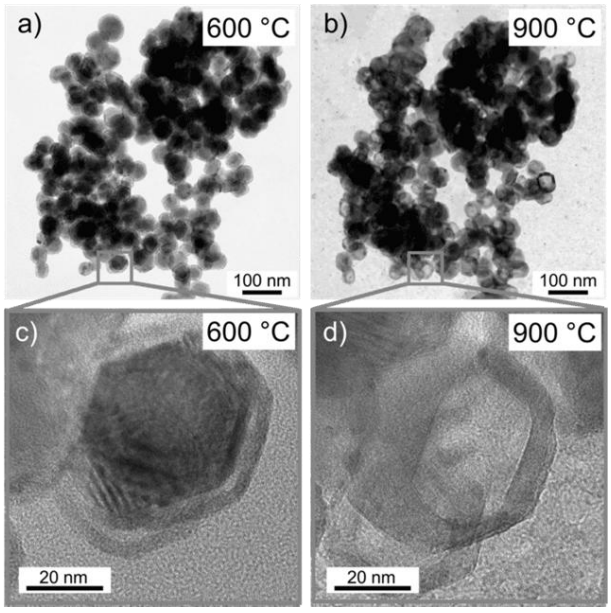

Fig. 6 *STEM BF images of the nanoparticles annealed to temperatures 300 – 900 °C*

To exclude beam-induced effects on shell thickening, we examined regions that were not exposed to the electron beam during annealing (Figure 7). As in the previously observed areas, hollow shells were present, ruling out beam exposure as the cause.

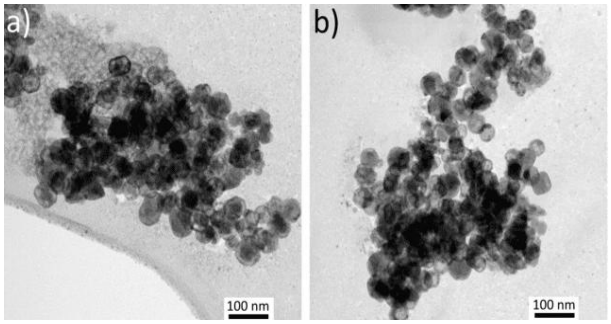

Fig. 7 *STEM BF after the annealing – areas which were not irradiated by the electron beam*

The specimens were also annealed in air at 500 °C, and the results are shown in Figure 8. Partial crystallization of the shell is observed, with anatase domains confirmed in selected regions. The particle separation and the formation of a clear interfacial gap occur, as also seen during in-situ annealing under vacuum. The oxidizing environment promotes more pronounced shell growth (~15 nm) compared to vacuum, while oxidation remains confined to the shell rather than extending into the core.

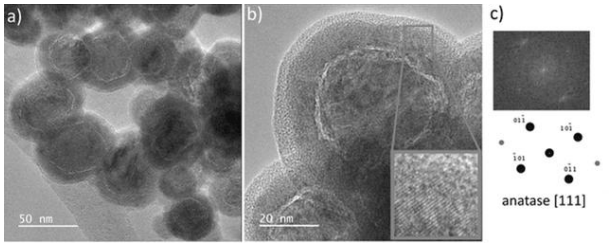

Fig. 8 *TEM images of the specimen annealed in air at 500 °C: (a) bright-field TEM, (b) high-resolution TEM, and (c) FFT from the orange-marked region, compared with a JEMS-simulated diffraction pattern of anatase along the [111] zone axis*

4 Discussion

In our experiments, Ti nanoparticles quickly form a TiO_x shell: the shell is amorphous at low temperatures, locally crystallizes to anatase in air at 500 °C (Figure 8), and by 600 °C, rutile is identified through HRTEM/FFT (Figure 5a–d). The oxide shell prevents coalescence at higher temperatures. Additionally, for TiO_2, the characteristic surface-diffusion sintering time at around 900 °C for approximately 50 nm particles is much longer than our dwell time, so the particles stay separate [29, 30].

The shell thickens (≈4 and ≈5 nm between RT and 600 °C) while the core shrinks (≈45 and ≈43 nm), and a clear interfacial gap forms (Figure 4), indicating ongoing oxidation of the core and its transformation into a TiO_2 shell. To evaluate whether a Kirkendall mechanism explains the observed void formation,

the following criterion can be used [31].

$$\frac{y \cdot D_{Ti} \cdot |\Delta C_{Ti}|}{x \cdot D_O \cdot |\Delta C_O|} + 1 > \frac{r_{out}^3(t) - r_{in}^3(t)}{r_{in}^3(t)} \quad (1)$$

Where:

D_{Ti}, D_O…Diffusion coefficients of Ti and O in TiO_2,

ΔC_{Ti}, ΔC_O…The corresponding concentration differences,

r_{out}, r_{in}…The positions of the outer and inner boundaries of the product layer at time t.

Once this criterion is satisfied, the difference in atomic migration rates between the core and shell materials becomes sufficiently large to drive the formation of the central void. Using r_{in}=15 nm and r_{out}= 20 nm together with extrapolated literature diffusion coefficients at 600 °C, where voiding is observed: $D_O \sim 10^{-22} m^2 s^{-1}$ [32] and D_{Tia} $\sim 5 \times 10^{-21} m^2 s^{-1}$ D_{Tic} $\sim 2 \times 10^{-19} m^2 s^{-1}$ [33], since $D_{Ti} >> D_O$, the inequality required by Eq. (1) is satisfied and therefore supporting differential-diffusion-driven hollowing under our conditions.

Regions not irradiated during in-situ annealing show the same shell separation and hollow morphology (Figure 7), and ex-situ air anneals reproduce this trend, indicating that electron-beam exposure is not the main cause in our system. We note that beam-induced oxidation and hollowing have been reported in other materials; for example, Xu et al. [34] observed In nanoparticles transforming into hollow InO_3 under electron irradiation in high vacuum—but our results show this effect also happens without beam exposure. Oxidation under nominal TEM high vacuum is plausible due to residual O_2/H_2O and possible oxygen release from the SiO_2 support; in all cases, oxidation stays confined to the shell.

SAED from nanoparticle ensembles (Figure 5e) further shows both rutile and brookite rings, consistent with a rutile/brookite assemblage in this temperature range. Rutile TiO_2 nanoparticles are widely used for dye-degradation photocatalysis, light-scattering layers in DSSC/QDSSC photoanodes, Li-ion battery anodes, and magnetically separable photocatalyst architectures [35–37]. The approximately 50 nm hollow TiO_2 shells reported here are well suited for photocatalysis and gas sensing—where their hollow structure provides high surface area and short transport paths, and rutile–brookite junctions help with charge separation [38, 39]—as well as high-temperature catalytic supports, where compact walls and rutile's thermal stability help maintain morphology under heat [40]. With longer annealing or dwell times, the mixed brookite/rutile shell is expected to mainly transform into rutile, consistent with the well-known anatase/brookite → rutile transformation during extended heating [41]. It remains uncertain whether significant sintering will occur during this process; however, the long characteristic sintering times reported for ~50 nm TiO_2 at these temperatures suggest that notable coarsening or coalescence is unlikely under our annealing conditions [29, 30].

5 Conclusions

DC magnetron sputtering was used to create Ti–TiO_x core–shell nanoparticles, which were then examined through in situ TEM annealing. Sputtering produces Ti–TiO_x core–shell nanoparticles (~50 nm in diameter, with a ~4 nm oxide shell). During annealing, the shell begins to crystallize locally into anatase at 500 °C and transforms into a rutile/brookite mixture by approximately 600 °C. The shell thickens (~4 to ~5 nm at 600 °C), the metallic core shrinks, and an interfacial gap forms, eventually leading to fully hollow shells with ~20 nm walls after heating to 900 °C. A volume expansion from Ti to TiO_2 and a diffusion imbalance (Kirkendall effect) are consistent with oxidation-driven Kirkendall hollowing as the main mechanism. The hollow structure remains stable up to 900 °C without significant coalescence. Experiments in beam-off regions and with ex-situ air annealing show the same evolution, indicating a thermally driven, not beam-induced, transformation that can be reliably reproduced in air. This method provides access to sub-50 nm, compact TiO_2 hollow shells with potential uses in photocatalysis, gas sensing, and high-temperature catalytic supports.

Acknowledgement

We acknowledge the funding and support from the Czech Science Foundation, grant number 22-22572S.

References

[1] WANG, D.; SONG, C.; LIN, Y.; HU, Z. (2006). Preparation and characterization of TiO_2 hollow spheres. In: *Materials Letters*, Vol. 60, No. 1, pp. 77–80.

[2] CARUSO, F. (2000). Hollow capsule processing through colloidal templating and self-assembly. In: *Chemistry – A European Journal*, Vol. 6, No. 3, pp. 413–419.

[3] ZHONG, Z.; YIN, Y.; GATES, B.; XIA, Y. (2000). Preparation of mesoscale hollow spheres of TiO_2 and SnO_2 by templating against crystalline arrays of polystyrene beads. In: *Advanced Materials*, Vol. 12, No. 3, pp. 206–209.

[4] ŠULCOVÁ, J., PAPUČOVÁ, I., PAGÁČOVÁ, J., DUBEC, A., FERIANCOVÁ, A., SUKEĽ, M. DEDINSKÝ PETER (2024). The Effect of TiO_2 Layers on

the Surface Properties of Materials. In: *Manufacturing Technology Journal*, Vol. 24, No. 2, pp. 272–278.

[5] COULTER, K.E.; SAULT, A.G. (1995). Effects of activation on the surface properties of silica-supported cobalt catalysts. In: *Journal of Catalysis*, Vol. 154, No. 1, pp. 56–64.

[6] WANG, A., ZHANG, H., LI, X., ZHANG, X., WANG, W. (2023). Method for Controlling Production Cost of Nano Ti-based Materials Based on DMAIC. In: *Manufacturing Technology*, Vol. 23, No. 3, pp. 354–365.

[7] ESKANDARLOO, H.; ZAFERANI, M.; KIERULF, A.; ABBASPOURRAD, A. (2018). Shape-controlled fabrication of TiO_2 hollow shells toward photocatalytic application. In: *Applied Catalysis B: Environmental*, Vol. 227, pp. 519–529.

[8] CHANDRA, M.; PRADHAN, D. (2020). Engineering the morphology and crystal phase of 3D hierarchical TiO_2 with excellent photochemical and photoelectrochemical solar water splitting. In: *ChemSusChem*, Vol. 13, pp. 3005–3016.

[9] KAVAN, L.; GRÄTZEL, M.; GILBERT, S.E.; KLEMENZ, C.; SCHEEL, H.J. (1996). Electrochemical and photoelectrochemical investigation of single-crystal anatase. In: *Journal of the American Chemical Society*, Vol. 118, No. 28, pp. 6716–6723.

[10] PFEIFER, V.; ERHART, P.; LI, S.; RACHUT, K.; MORASCH, J.; BRÖTZ, J.; RECKERS, P.; MAYER, T.; RÜHLE, S.; ZABAN, A.; MORA-SERÓ, I.; BISQUERT, J.; JAEGERMANN, W.; KLEIN, A. (2013). Energy band alignment between anatase and rutile TiO_2. In: *Journal of Physical Chemistry Letters*, Vol. 4, No. 23, pp. 4182–4187.

[11] HORKÝ, R., KUŚMIERCZAK, S., NÁPRSTKOVÁ, N., KAMBAROVÁ, I. (2024). Effect of Heat Treatment and Corrosion Load on the Microstructure of the Ti6Al4V Alloy. In: *Manufacturing Technology*, Vol. 24, No. 6, pp. 914–928.

[12] IMHOF, A.; PINE, D.J. (2001). Preparation and characterization of titania-coated polystyrene spheres and hollow titania shells. In: *Langmuir*, Vol. 17, pp. 3579–3585.

[13] BAO, Y.; et al. (2018). Sol-gel-controlled synthesis of hollow TiO_2 spheres and their photocatalytic properties. In: *Materials Letters*, Vol. 222, pp. 266–269.

[14] HANPRASOPWATTANA, A.; et al. (1996). Titania coatings on monodisperse silica spheres… In: *Langmuir*, Vol. 12, pp. 3173–3179.

[15] MAHONEY, L.; KOODALI, R.T. (2014). Versatility of evaporation-induced self-assembly (EISA) method for preparation of mesoporous TiO_2 for energy and environmental applications. In: *Materials*, Vol. 7, pp. 2697–2746.

[16] WANG, Y.; et al. (2008). Preparation of TiO_2 hollow microspheres by the reverse microemulsion method. In: *Materials Letters*, Vol. 62, pp. 3801–3804.

[17] CHEN, T.; et al. (2007). Organic–inorganic hybrid hollow spheres prepared from a TiO_2 -stabilized Pickering emulsion polymerization. In: *Advanced Materials*, Vol. 19, pp. 4537–4541.

[18] OKANOVIĆ, V.; et al. (2004). Designing of nanostructured hollow TiO_2 spheres obtained by ultrasonic spray pyrolysis. In: *Materials Science and Engineering B*, Vol. 112, pp. 173–178.

[19] LONG, L.; et al. (2015). Ammonia-cation-assisted oxygen bubble template for hollow TiO_2 nanospheres. In: *RSC Advances*, Vol. 5, pp. 112830–112836.

[20] YANG, H.G.; ZENG, H.C. (2004). Preparation of hollow anatase TiO_2 nanospheres via Ostwald ripening. In: *Journal of Physical Chemistry B*, Vol. 108, No. 11, pp. 3492–3495.

[21] LIANG, J.; HAN, X.; LI, Y.; YE, K.; HOU, C.; YU, K. (2015). Fabrication of TiO_2 hollow nanocrystals through the nanoscale Kirkendall effect for lithium-ion batteries and photocatalysis. In: *New Journal of Chemistry*, Vol. 39, No. 4, pp. 3145–3149.

[22] WANG, L.; et al. (2002). Fabrication of controllable ultrathin titania hollow shells by LbL of titania nanosheets on polymer templates. In: *Chemistry of Materials*, Vol. 14, pp. 4827–4832.

[23] LEE, W.-J.; HON, M.-H.; CHUNG, Y.-W.; LEE, J.-H. (2011). A three-dimensional nanostructure consisting of hollow TiO_2 spheres fabricated by template-assisted atomic layer deposition. In: *Japanese Journal of Applied Physics*, Vol. 50, No. 6GH06.

[24] TANG, Y.; YANG, L.; CHEN, J.; QIU, Z. (2010). Facile fabrication of hierarchical hollow microspheres assembled by titanate nanotubes. In: *Langmuir*, Vol. 26, No. 12, pp. 9722–9725.

[25] ZHANG, J.; CHOI, S.-W.; KIM, S.-S. (2011). Micro- and nano-scale hollow TiO_2 fibers by coaxial electrospinning. In: *Journal of Solid State Chemistry*, Vol. 184, pp. 3008–3013.

[26] YU, K.; LING, M.; LIANG, J.; LIANG, C. (2019). Formation of TiO_2 hollow spheres through nanoscale Kirkendall effect and their lithium storage and photocatalytic properties. In: *Chemical Physics*, Vol. 517, pp. 222–227.

[27] LI, X.; LI, M.; LIANG, J.; WANG, X.; YU, K. (2016). Growth mechanism of hollow TiO_2(B) nanocrystals as powerful application in lithium-ion batteries. In: *Journal of Alloys and Compounds*, Vol. 681, pp. 471–476.

[28] ZURMÜHL, C.; POPESCU, R.; GERTHSEN, D.; FELDMANN, C. (2011). Microemulsion-based synthesis of nanoscale TiO_2 hollow spheres. In: *Solid State Sciences*, Vol. 13, No. 8, pp. 1505–1509.

[29] KOBATA, A.; KUSAKABE, K.; MOROOKA, S. (1991). Growth and transformation of TiO_2 crystallites in aerosol reactor. In: *AIChE Journal*, Vol. 37, No. 3, pp. 347–359.

[30] BUESSER, B.; GRÖHN, A. J.; PRATSINIS, S. E. (2011). Sintering rate and mechanism of TiO_2 nanoparticles by molecular dynamics. In: *Journal of Physical Chemistry C*, Vol. 115, No. 22, pp. 11030–11035.

[31] YANG, Z.; YANG, N.; PILENI, M.-P. (2015). Nano Kirkendall effect related to nanocrystallinity of metal nanocrystals: Influence of the outward and inward atomic diffusion on the final nanoparticle structure. In: *Journal of Physical Chemistry C*, Vol. 119, No. 39, pp. 22249–22260.

[32] DENNIS, P.F.; FREER, R. (1993). Oxygen self-diffusion in rutile under hydrothermal conditions. In: *Journal of Materials Science*, Vol. 28, No. 18, pp. 4804–4810.

[33] LUNDY, T.S.; COGHLAN, W.A. (1973). Cation self diffusion in rutile. In: *Journal de Physique Colloques*, Vol. 34, No. C9, pp. 299–302. (Proceedings of the European Physical Society Topical Conference Lattice Defects in Ionic Crystals, Marseille-Luminy, France, July 2–6, 1973).

[34] XU, T.; ZHANG, H.; YE, M.; ZHU, Y.; YUAN, D.; LI, W.; ZHOU, Y.; SUN, L. (2022). Controllable fabrication of hollow In_2O_3 nanoparticles by electron beam irradiation. In: *Nanoscale*, Vol. 14, pp. 12569–12573.

[35] ZHOU, Z.; YIN, H.; ZHAO, Y.; ZHANG, J.; LI, Y.; YUAN, J.; TANG, J.; WANG, F. (2021). Synthesis of magnetic α-Fe_2O_3/rutile TiO_2 hollow spheres for visible-light photocatalytic activity. In: *Catalysts*, Vol. 11, No. 3, Art. 396.

[36] JIAO, S.; LIAN, G.; JING, L.; XU, Z.; WANG, Q.; CUI, D.; WONG, C.-P. (2018). Sn-doped rutile TiO_2 hollow nanocrystals with enhanced lithium-ion batteries performance. In: *ACS Omega*, Vol. 3, No. 1, pp. 1329–1337.

[37] WANG, H.; MIYAUCHI, M.; ISHIKAWA, Y.; PYATENKO, A.; KOSHIZAKI, N.; LI, Y.; LI, L.; LI, X.; BANDO, Y.; GOLBERG, D. (2011). Single-crystalline rutile TiO_2 hollow spheres: Room-temperature synthesis, tailored visible-light-extinction, and effective scattering layer for quantum dot-sensitized solar cells. In: *Journal of the American Chemical Society*, Vol. 133, No. 47, pp. 19102–19109.

[38] JUSTH, N.; BAKOS, L. P.; HERNÁDI, K.; KISS, G.; RÉTI, B.; ERDÉLYI, Z.; PARDITKA, B.; SZILÁGYI, I. M. (2017). Photocatalytic hollow TiO_2 and ZnO nanospheres prepared by atomic layer deposition. In: *Scientific Reports*, Vol. 7, Article 4337.

[39] XU, H.; ZHANG, L.Z. (2009). Controllable one-pot synthesis and enhanced photocatalytic activity of mixed-phase TiO_2 nanocrystals with tunable brookite/rutile ratios. In: *Journal of Physical Chemistry C*, Vol. 113, No. 5, pp. 1785–1790.

[40] TIAN, X.; CUI, X.; LAI, T.; REN, J.; YANG, Z.; XIAO, M.; WANG, B.; XIAO, X.; WANG, Y. (2021). Gas sensors based on TiO_2 nanostructured materials for the detection of hazardous gases: A review. In: *Nano Materials Science*, Vol. 3, No. 4, pp. 390–403.

[41] HANAOR, D.A.H.; SORRELL, C.C. (2011). Review of the anatase to rutile phase transformation. In: *Journal of Materials Science*, Vol. 46, pp. 855–874.